A study on exit burr formation in grinding process - Simulation and experiment

Gongyu Liu[a], Ming Chen[b, *], Qinglong An[c], Weiwei Ming[d],Jinyang Xu[e]

School of Mechanical Engineering, Shanghai Jiao Tong University, 200240, Shanghai, China

[a] yuzhongdesong@sjtu.edu.cn, [b]mchen@sjtu.edu.cn, [c]glan@sjtu.edu.cn, [d]mingseas@163.com, [e]xujinyang@sjtu.edu.cn

Keywords: Exit burr formation; FE simulation; Grinding process; Grinding conditions

Abstract. Exit burrs are easily generated on workpiece edges. Particularly, in grinding process, they could deteriorate the highly required precision and even affect the functionality of components**.** Therefore, to understand the burr formation mechanism and control it in grinding process becomes of great significance. To this end, this paper investigates the features and mechanism of exit burr formation, as well as the influence of grinding conditions (grain size, grinding speed, grinding depth) on the exit burr formation on stainless steel (12CrMoV) using the grinding wheels (SiC). A 3D finite element (FE) model of single grain grinding process was developed for explaining the exit burr formation procedures. Based on which, effects of grinding conditions on burr sizes were also studied. Simulation results were validated by a series of grinding trials and the following optical observations with the metallographic specimens of workpiece edges. It was found that the procedure of exit burr formation could be divided into four stages: pre-initiation, plastic bending occurrence, plastic deformation band formation, and burr development. The burr length was strongly determined by the grain size and grinding depth, rather than the grinding speed.

Introduction

Burrs formed in the grinding process could deteriorate the highly required precision of edge geometry in many industries [1]. The material deformation imposed by abrasive grains on the grinding wheel, especially at the workpiece edges, always results in the generation of micro- or macroscopic burrs. However, to avoid burrs completely in material removal process is still impossible on the current techniques level [2], it is regarded as a practical approach to control the burr formation in grinding process, so as to create acceptable burrs which will either meet the manufacturing requirements of the workpiece, or facilitate the subsequent deburring process greatly [3]. To this end, understanding the burr formation mechanism and on which the effects of process conditions becomes of great importance.

In the typical finishing operation of grinding, high requirements are usually put forward on the precision of edge geometries of parts. However, exit burr formation is the most problematic aspect facing the grinding process, which needs to be investigated and minimized for improving the part quality. Towards the burr formation in the grinding operation, only a few previous contributions have been done through experiments or simulations. Aurich et al. [3] carried out the experiments of flat surface grinding with tempered steel, based on which they proposed a descriptive model of burr formation in grinding. The model can be subdivided into the steps of continuous grinding, pre-initiation, burr initiation, burr development and final burr formation. Fu et al. [4] studied the formation mechanism and geometry characteristics of exit burrs in surface grinding of Ti-6Al-4V by performing the 2D FE simulation. They observed that the parameter combination of higher grinding speed, smaller uncut chip thickness, and

smaller rake angle of CBN grain could contribute to the easy removal of positive burrs. However, there is still a lack of persuasion among the research methods or conclusions in aforementioned literature, because: (1) the descriptive model could hardly provide quantitative evidence for precisely controlling the formation and subsequent removal of the burrs, and (2) the 2D FE model could hardly provide the accurate description of the practical 3D machining condition of the grinding process. In comparison of the common cutting processes, the distinctive characteristics of a high forward velocity, a low depth of cut, and a negative rake angle of grits are detected in the grinding process. Therefore, the burr shapes and formation mechanisms could be different from those in the cutting processes.

To better understand the burr formation in grinding process, this paper utilizes the combined FE simulation and experimental investigation to study the burr formation mechanisms and the effects of grinding conditions on burr sizes. Due to the fact that the exit burr is generally the largest in size among burrs at other locations [5], attentions will be paid to the formation of the exit burr. Since the single grit broaching simulation is easy to be performed and has shown admirable prediction results [6], the 3D FE model is developed to give clear descriptions of the burr formation procedures when the grit is moving out of the workpiece. The experiments of end face grinding on 12CrMoV stainless steel are carried out, to validate the applicability of the FE model and demonstrate the variations of burr sizes with different grinding conditions.

Process of Exit Burr Formation in Grinding

FE Simulation Modeling. To explain the exit burr formation procedures, 3D FE models of the single grain grinding process were developed based on the DEFORM-3D software. The equivalent rake angle θ and tip radius r of the grits (as shown in Fig. 1) were statistically measured and listed in Table 1, based on the three types of SiC grinding wheels to be used in the following experiments. The workpiece material was 12CrMoV stainless steel, which was the same as that used in the experiments. The grit was set in a rigid type, while the workpiece in a plastic type. The workpiece was modeled with a rectangle shape with dimensions of 150 × 100 × 40 μm^3. As shown in Fig. 2, the tetrahedral grids were applied to both the grit and the workpiece, whose total numbers of elements were 8743 and 55124, respectively. The grit moved through the stationary workpiece with process parameters listed in Table 2.

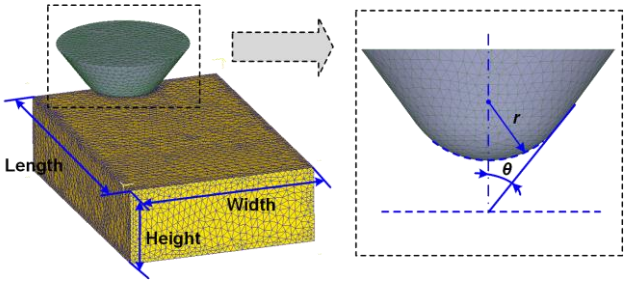

Fig. 1. The grit and workpiece for the single grit grinding simulation

Table 1 Geometrical results of measured grits

Wheel type, d	80#	100#	120#
θ [°]	42	40	38
r [μm]	36	27	25

Table 2 Process parameters for simulations

Parameters	Grinding speed v [m/s]	Grinding depth a_g [μm]	Grit size (Wheel granularity) d

Values	24, 30, 36	2, 4, 6, 8, 10, 15	80#, 100#, 120#

In this investigation, the Johnson-Cook (JC) constitutive model was used as presented by Eq. 1,

$$\sigma = (\mathrm{A} + \mathrm{B}\varepsilon^{\mathrm{n}})\left(1 + \mathrm{C}\ln\frac{\dot{\varepsilon}}{\dot{\varepsilon}_0}\right)\left[1 - \left(\frac{\mathrm{T}-\mathrm{T_r}}{\mathrm{T_m}-\mathrm{T_r}}\right)^{\mathrm{m}}\right]. \quad (1)$$

where ε is the equivalent plastic strain; $\dot{\varepsilon}$ and $\dot{\varepsilon}_0$ (1/s) are the equivalent and reference plastic strain rates, respectively; T (ºC) is the material temperature of the cutting zone; T_m (ºC) is the melting temperature; T_r (ºC) is the room temperature; n is the strain hardening index; m is the thermal softening index; A (Mpa), B (Mpa), and C are the material constants. These coefficients obtained by Gupta et al. [7] are used for the simulations as summarized in Table 3.

Table 3 Coefficients of the JC model for the workpiece material [7]

Coefficients	A [MPa]	B [MPa]	C	m	n	$\dot{\varepsilon}_0$ [1/s]	T_m [ºC]	T_r [ºC]
Values	209.7	1383.2	-0.0095	0.5147	0.915	0.01	1400	20

Besides, the Johnson-Cook (JC) damage model was adopted as the ductile failure criterion of the workpiece material in the simulations, as described by Eq. 2,

$$\dot{\varepsilon}_f = \left[d_1 + d_2\exp\left(d_3\frac{p}{q}\right)\right]\left[1 + d_4\ln\left(\frac{\dot{\varepsilon}}{\dot{\varepsilon}_0}\right)\right]\left(1 + d_5\left(\frac{T-T_r}{T_m-T_r}\right)\right). \quad (2)$$

where $d_1 \sim d_5$ are the constant parameters, p (Mpa) is the hydrostatic pressure, q (Mpa) is the Mises stress, $\dot{\varepsilon}_0$ is the reference strain rate, and $\dot{\varepsilon}$ is the strain rate at the time of failure. These constants given by Pham and Iwamoto [8] are used for the simulations as listed in Table 4.

Table 4 Coefficients of the JC damage criteria for the workpiece material [8]

Coefficients	d_1	d_2	d_3	d_4	d_5
Values	2.0	1.936	-2.969	-0.06	1.014

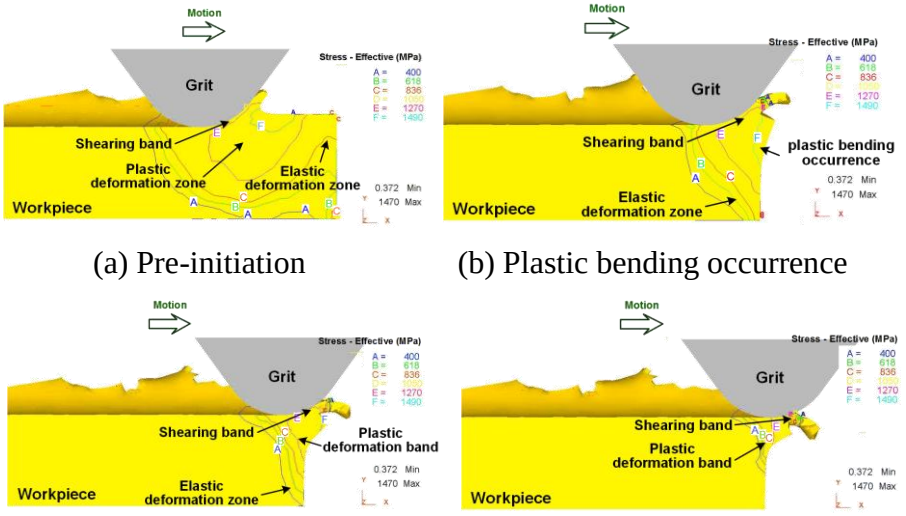

(a) Pre-initiation (b) Plastic bending occurrence

(c) Plastic deformation band formation (d) Burr development

Fig. 2. The procedures of the exit burr formation

Exit Burr Formation Procedures. The exit burr formation procedures obtained from the FE simulations are shown in Fig. 2. It can be found that there are mainly four procedures during

the exit burr formation: pre-initiation, plastic bending occurrence, plastic deformation band formation, and burr development. In the pre-initiation procedure, the grit moves near the workpiece edge, an elastic deformation zone firstly appears, and then extends to the workpiece margin in the form of bending. Meanwhile, the plastic deformation at the primary shear zone extends rapidly to the side face of workpiece. The stress and strain distribution has been affected obviously by the side face. In the plastic bending occurrence procedure, a small plastic deformation zone suddenly occurs on the side face, resulting in the downward bending of the workpiece edge. The occurrence of this deformation zone indicates that the real interaction depth of the grit with the workpiece starts to decrease gradually. Therefore, the proportion of the compression component becomes larger, and the burr begins to rotate to some degrees. In the plastic deformation band formation procedure, the plastic deformation at the primary shear zone extends to and finally connects with the plastic bending occurrence zone on the side face. Then, the continuum zone of the plastic shearing band emerges near the workpiece edge, which spatially separates the workpiece material into two parts. This deformation band has a strong influence on the strength distribution of the edge and the deburring process afterwards. In the burr development procedure, the material at the workpiece edge is pushed by the grit and slides outwards and downwards along the plastic deformation band, and the burr size increases significantly. Finally, the exit burr is generated.

Experimental Setup

The end face grinding trials were performed using the grinding machine of STUDER S20, as shown in Fig. 3(a). The vitrified bond grinding wheels with SiC grits were used in the trials. The wheel hardness grade was medium soft K, and the wheel structure grade was medium 7. The wheel granularities used for the trials included 80#, 100#, and 120#. The wheel sizes were $\Phi 350 \times 32 \times \Phi 127$ mm^3. The burr sizes measured in this investigation include the burr width w, the height of burr root part h_1, and the height of burr rollover part h_2, as shown in Fig. 3(b).

In this investigation, we totally prepared five workpiece specimens at the same conditions for each trial, and then took them to be sliced by the electrical discharge machining process. The slicing direction was perpendicular to the workpiece edges where the grits moved out of the workpieces. After that, the specimens were mounted into the thermosetting resins carefully, and taken to be polished by the polishing machine until the exit burr on each workpiece edge could be observed clearly by the optical microscope (Keyence VHX-600). Then, the burr sizes on the samples made at the same experimental conditions were statistically measured using the microscope, and the average burr sizes were calculated for minimizing the random errors.

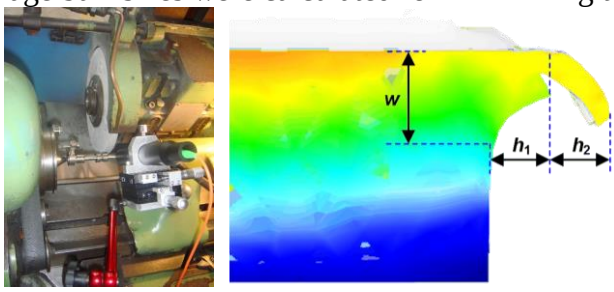

Fig. 3. (a) Experimental setup, (b) Measurement of burr sizes.

Effects of Grinding Conditions on Burr Sizes

Grinding Speed. From Fig. 4, it can be seen that the variation trend of the burr size obtained from experiments is similar to that from simulations. With the increase of the grinding speed, the height of the burr root part h_1, the height of the burr rollover part h_2, and the burr width w

change differently. As for h_1, it decreases firstly and then increases; as for h_2, it increases slowly and linearly; as for w, it changes oppositely with h_2. When the grinding speed increases, the heat generated in the process also increases, and the grinding force decreases. Firstly, h_1 decreases due to the smaller grinding force, then, it gradually increases as the temperature increases and plays the dominant role. As for h_2, the increase of the grinding speed could contribute to the increase of the material deformation strain rate, and decreases the chip deformation coefficient, therefore, h_2 increases. As for w, because the grinding force has a dominant effect on it, the decrease of the grinding force causes a smaller burr width w.

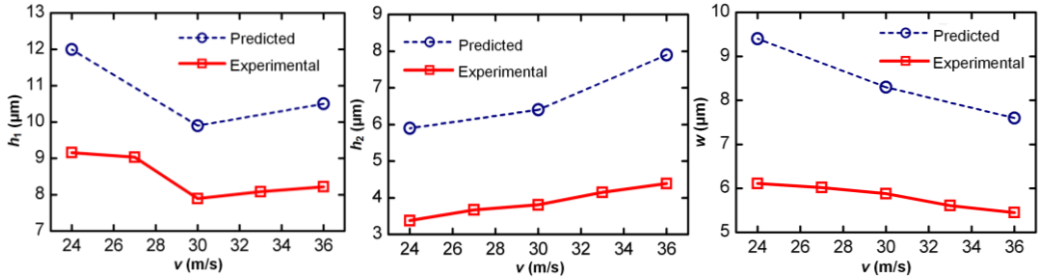

Fig. 4. Effects of the grinding speed on exit burr sizes

Grinding Depth. Fig. 5 shows the effect of the grinding depth on exit burr sizes. It is clear that the experimental results have the same trend as the simulation, which indicates the validity of the FE simulations in this study. When the grinding depth increases, the height of the burr root part h_1 increases approximately linearly, while the height of the burr rollover part h_2 and the burr width w increase rapidly first and then slowly. As is known, the larger grinding depth could induce the larger grinding force, and the plastic deformation zone of the material will be enlarged. This effect could definitely result in the increase of burr sizes. However, it is worth noting that the mismatch between the predicted w and the experimental w when a_g = 0.015 mm still needs to be further studied.

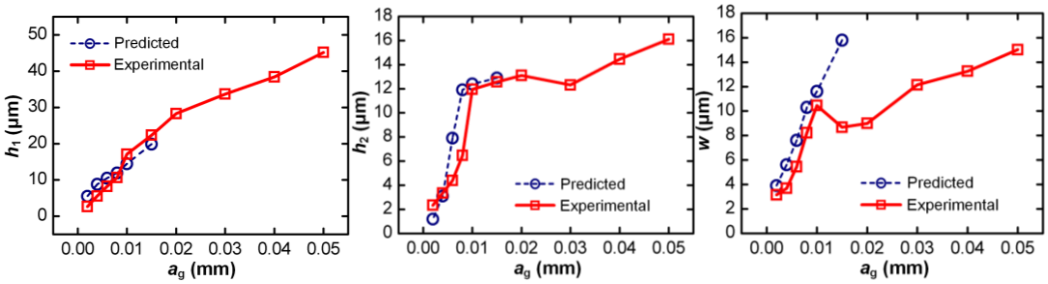

Fig. 5. Effects of the grinding depth on exit burr sizes

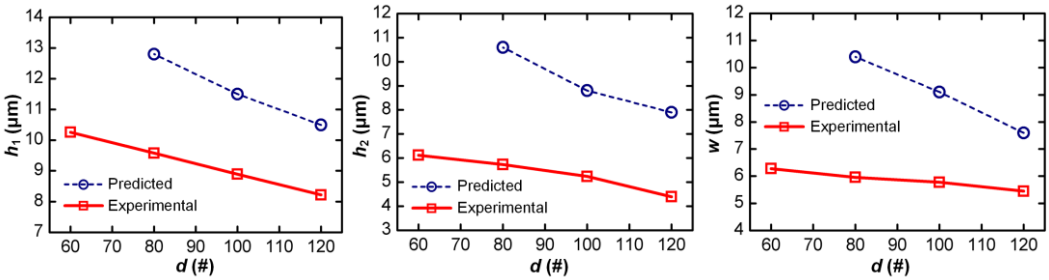

Fig. 6. Effects of the wheel granularity (grit size) on exit burr sizes

Wheel Granularity (Grit Size). Fig. 6 shows the effect of the grit size on exit burr sizes. As can be seen from the figure, the variation trend of the predicted burr sizes is similar to the experimental results. With the increase of the wheel granularity (decrease of the grit size), all the heights and the width of burrs decrease gradually. When the grit becomes smaller, both the

equivalent rake angle θ and tip radius r decreases. Thus, the amount of plastically deformed material resulting from the movement of the grit would also be reduced, which leads to the decrease of exit burr sizes. It is worth noting that the simulation results are larger than the experimental ones. This is because that the boundaries given for simulations have limitations to be exactly the same as the complicated grinding process in real.

Summary

This paper investigated the mechanisms of the exit burr formation based on 3D FE simulations of the single grit grinding process. Simulation results showed that the exit burr formation mainly included four stages: the pre-initiation, the plastic bending occurrence, the plastic deformation band formation, and the burr development. Then, experiments were carried out to investigate the effects of grinding conditions including the grinding speed, grinding depth, and grit size (grinding wheel granularity) on exit burr sizes. Experimental results showed that, with the variations of grinding conditions, the height of the burr root part h_1, the height of the burr rollover part h_2, and the burr width w changed differently. Generally, the burr sizes were more strongly determined by the grit size and grinding depth than the grinding speed. This investigation is beneficial for the exit burr minimization and improvement of the workpiece quality.

Acknowledgement

This work is supported by Important National Science & Technology Specific Projects (2017ZX04016001).

References

[1] I. A. Choudhury, and S. A. Lawal, Burr formation in machining processes: a review, Refer. Mod. Mater. Sci. Mater. Eng. 11 (2014) 283-295.

[2] P. T. Blotter, and L. K. Gillespie, The formation and properties of machining burrs, T. ASME 98 (1976) 66-74.

[3] J. C. Aurich, H. Sudermann and H. Bil, Characterization of burr formation in grinding and prospects for modelling, CIRP Ann. 54 (2005) 313-316.

[4] D. Fu, W. Ding, S. Yang, Q. Miao and Y. Fu, Formation mechanism and geometry characteristics of exit-direction burrs generated in surface grinding of Ti-6Al-4V titanium alloy, Int. J. Adv. Manuf. Tech. 89 (2016) 2299-2313.

[5] R. Dollmeier, C. Barth, and G. Warnecke, Burr formation in grinding of hardened steel with conventional and superabrasive wheels, T. ASME 29 (2001) 273-278.

[6] G. Guerrini, A. A. G. Bruzzone, and F. Crenna, Single grain grinding: an experimental and FEM assessment, Procedia CIRP 62 (2017) 287-292.

[7] A. K. Gupta, H. N. Krishnamurthy, Y. Singh, K. M. Prasad and S. K. Singh, Development of constitutive models for dynamic strain aging regime in austenitic stainless steel 304, Mater. Design 45 (2013) 616-627.

[8] H. T. Pham and T. Iwamoto, An evaluation of fracture properties of type-304 austenitic stainless steel at high deformation rate using the small punch test, Int. J. Mech. Sci. 144 (2018) 249-261.